Supplemental Material

I. FURTHER DETAILS OF THE MODEL

Supplemental Table I. **Numerical parameters in the model.** Parameterized according to Eq. (1) in the main text. Zeroes are omitted from the table for clarity.

Bond (i)	$\tau^{(i)}$	$\lambda_1^{(i)}$	$\lambda_2^{(i)}$	$\lambda_3^{(i)}$
1	-0.7	-0.4	-0.2	
2		-0.6		-1.0
3	-0.3	-0.7	-0.4	
4		0.9	0.3	
5	-0.2	0.4	0.3	
6	-3.0	-2.1	1.2	
7	0.5	1.2	-0.7	

While Eqs. (1) and (2) in the main text, together with the numerical parameters in Supplemental Table I, fully determine our model, for readers' convenience we present below an explicit matrix form of $\hat{H}_0$. To achieve that, we first specify our coordinate system. Let a be the lattice constant, and let $\{\boldsymbol{a}_i\}$ and $\{\boldsymbol{b}_i\}$ respectively be the primitive lattice vectors and the corresponding reciprocal lattice vectors. We pick

$$\begin{aligned}\boldsymbol{a}_1 =& a\left(\frac{\sqrt{3}}{2}\hat{x}-\frac{1}{2}\hat{y}\right);\quad \boldsymbol{a}_2 = a\,\hat{y};\\ \boldsymbol{b}_1 =& \frac{4\pi}{\sqrt{3}a}\hat{x};\quad \boldsymbol{b}_2 = \frac{4\pi}{\sqrt{3}a}\left(\frac{1}{2}\hat{x}+\frac{\sqrt{3}}{2}\hat{y}\right).\end{aligned} \tag{S1}$$

The honeycomb sites are at $\boldsymbol{r}_1 = \boldsymbol{a}_1/3 + 2\boldsymbol{a}_2/3$ and $\boldsymbol{r}_2 = 2\boldsymbol{a}_1/3 + \boldsymbol{a}_2/3$ (matrix indexing of the sites proceeds in that order). We parameterize the BZ by $\boldsymbol{k} = (g_1\boldsymbol{b}_1 + g_2\boldsymbol{b}_2)/2\pi$, where $g_i \in (-\pi, \pi]$.

We expand the Bloch Hamiltonian for $\hat{H}_0$ as

$$H_0(g_1, g_2) = \frac{t}{12}\sum_{i,j=0}^{3} h_{ij}(g_1, g_2)\,\sigma_i \otimes \sigma_j, \tag{S2}$$

where the first set of Pauli matrices corresponds to the site degrees of freedom, the second set is for the spin, and

$$\begin{aligned}
h_{00} =& -\frac{4}{5}(\cos(g_1-g_2)+\cos(2g_1+g_2)+\cos(g_1+2g_2));\\
h_{01} =& \frac{3}{5}\left(2(\sin(g_1+g_2)-\sin g_1)-\left(4+\sqrt{3}\right)\sin\left(\frac{3g_2}{2}\right)\cos\left(g_1+\frac{g_2}{2}\right)+4\sin g_2\right);\\
h_{02} =& \frac{1}{5}\sin\left(g_1+\frac{g_2}{2}\right)\left(\left(6+8\sqrt{3}\right)\left(\cos\left(g_1+\frac{g_2}{2}\right)+\cos\left(\frac{g_2}{2}\right)\cos g_2\right)-\left(3+16\sqrt{3}\right)\cos\left(\frac{g_2}{2}\right)\right);\\
h_{10} =& \frac{2}{5}(3\sin g_1\sin g_2-9\cos g_1\cos g_2-7(\cos g_1+\cos g_2+1));\\
h_{11} =& \frac{3-\sqrt{3}}{10}(3\sin(2g_1)-2\sin(g_2)-3\sin(2g_1+g_2))+\frac{21+4\sqrt{3}}{5}\cos(g_1)\sin(g_2)-\frac{3(3+\sqrt{3})}{5}\sin(g_2)\cos(g_1+g_2)\\
&-\frac{9}{5}\sin(2g_2);\\
h_{12} =& \frac{3\left(1+3\sqrt{3}\right)}{10}\left(\sin(2g_1+g_2)+\sin(2g_1)\right)+\frac{3\left(3\sqrt{3}-1\right)}{10}\sin(g_1+2g_2)-\frac{4+7\sqrt{3}}{5}(2\sin g_1\cos g_2+\cos g_1\sin g_2)\\
&+\frac{\sqrt{3}-7}{10}\sin g_1-\frac{2\left(2+\sqrt{3}\right)}{5}\sin g_2+\frac{3}{5}\sin(2g_2);\\
h_{20} =& \frac{2}{5}(7(\sin g_2-\sin g_1)-3\sin(g_1-g_2));\\
h_{21} =& \frac{1}{10}\sin g_2\left(6\left(3+\sqrt{3}\right)\sin(g_1+g_2)+\left(42+8\sqrt{3}\right)\sin g_1+3\left(\sqrt{3}-3\right)\sin(2g_1)\right)\\
&+\frac{1}{5}\sin^2\left(\frac{g_2}{2}\right)\left(\left(\sqrt{3}-3\right)(3\cos(2g_1)-2)+36\cos g_2\right);\\
h_{22} =& -\frac{1}{5}\cos^2\left(\frac{g_2}{2}\right)\left(\left(3+9\sqrt{3}\right)\cos(2g_1)+4\left(\sqrt{3}+2-3\cos g_2\right)\right)+\frac{1}{5}\sin g_1\sin g_2\left(\left(3-9\sqrt{3}\right)\cos g_2+7\sqrt{3}+4\right)\\
&+\frac{1}{10}\cos g_1\left(6\left(1+3\sqrt{3}\right)\sin g_1\sin g_2+\left(9\sqrt{3}-3\right)\cos(2g_2)+17\sqrt{3}+1\right);\\
h_{33} =& 4(\sin g_1+\sin g_2-\sin(g_1+g_2)).
\end{aligned}$$

Note that the terms $h_{03}, h_{13}, h_{23}, h_{30}, h_{31}, h_{32}$ vanish, and are therefore omitted from the above.

We also write out the coupling Hamiltonian $\hat{H}_c$ in an explicit single-particle matrix form:

$$H_c(g_1,g_2)=\frac{c}{12}\begin{pmatrix}0 & 0 & C_{13}\\ 0 & 0 & C_{23}\\ C_{13}^\dagger & C_{23}^\dagger & 0\end{pmatrix}. \tag{S3}$$

Note that H_c is written in a block matrix form, with the index ordering corresponding to the following basis vectors in the unit cell: $\boldsymbol{r}_1$, $\boldsymbol{r}_2$ and $\boldsymbol{r}_3\equiv\mathbf{0}$. The 2×2 sub-matrices C_{13} and C_{23} are functions of (g_1,g_2), given by

$$\begin{aligned}
C_{13}=&\left[2\cos(g_1)-6\left(e^{i(g_1+g_2)}+e^{ig_2}+1\right)+e^{i(g_1+2g_2)}\right]\sigma_0\\
&+\frac{1}{20}\left[3\left(21+4\sqrt{3}\right)\left(\sin(g_2)-i\cos(g_2)+i\right)-2\left(36+7\sqrt{3}\right)e^{i(g_1+g_2)}\sin(g_2)\right]\sigma_1\\
&-\frac{1}{20}ie^{-ig_1}\left[\left(7+12\sqrt{3}\right)\left(e^{2i(g_1+g_2)}+e^{2ig_1}-2\right)+3\left(4+7\sqrt{3}\right)e^{ig_1}\left(1+\left(1-2e^{ig_1}\right)e^{ig_2}\right)\right]\sigma_2;\\
C_{23}=&\left[2\cos(g_2)-6\left(e^{i(g_1+g_2)}+e^{ig_1}+1\right)+e^{2ig_1+ig_2}\right]\sigma_0\\
&+\frac{1}{20}ie^{-ig_2}\left[\left(36+7\sqrt{3}\right)\left(e^{2ig_2}-1\right)+3\left(21+4\sqrt{3}\right)\left(1-e^{ig_2}\right)e^{i(g_1+g_2)}\right]\sigma_1\\
&+\frac{1}{20}ie^{-ig_2}\left[3\left(4+7\sqrt{3}\right)e^{ig_2}\left(e^{i(g_1+g_2)}+e^{ig_1}-2\right)+\left(7+12\sqrt{3}\right)\left(1+\left(1-2e^{2ig_1}\right)e^{2ig_2}\right)\right]\sigma_2.
\end{aligned}$$

One can check that the given Hamiltonians are indeed symmetric under the stated symmetries following the procedure delineated in, e.g., Ref. 18.

II. DEFORMATION TO AN EXPLICIT ATOMIC LIMIT

While the valence bands of $\hat{H}_0$ possess a full set of symmetric, exponentially localized Wannier functions—a property of the honeycomb model without the need for any additional degrees of freedom—a further check on their triviality concerns its deformability to an explicit atomic limit. To this end, we augment the electronic degrees of freedom in the model by an additional p_z orbital localized to each of the centers of the hexagons. These additional sites form a triangular lattice by themselves. As the problem is set up, initially, the wavefunctions of the valence bands of $\hat{H}_0$ have zero amplitude on these new sites. We then consider a Hamiltonian $\hat{H}_c$ which couples the two sets of lattice sites (Supplemental Fig. 1a). Combining $\hat{H}_c$ and $\hat{H}_0$ with a tunable relative strength between the two, we consider a continuous family of Hamiltonians $\{\hat{H}(\mu)\,:\,\mu\in[0,1]\}$ with the following properties: (i) All the stated symmetries are maintained for all μ; (ii) The honeycomb and triangular lattices are decoupled for $\mu=0$ or 1; (iii) the two lowest bands of $\mu=0$ are identical to those of $\hat{H}_0$; and (iv) the two lowest bands of $\mu=1$ arise solely from the triangular lattice sites. $\hat{H}(\mu)$ therefore interpolates between $\hat{H}_0$ and an explicit, strongly localized atomic limit in a symmetric manner.

Next, we construct $\hat{H}_c$ and $\hat{H}(\mu)$ explicitly. The coupling Hamiltonian $\hat{H}_c$ is defined in the same way as $\hat{H}_0$ in Eqs. (1) and (2) in the main text, except that we sum over bonds $i=6,7$, and replace the energy scale t by a μ-dependent coupling constant $c(\mu)=t\cos\left[(1-2\mu)\pi/2\right]$. Note that $c(0)=c(1)=0$. In addition, we add an additional chemical potential offset (measured with respect to the Fermi energy of $\hat{H}_0$) between the honeycomb and triangular lattices, captured by $\hat{H}_\triangle(\mu)=3(1-2\mu)t\hat{N}_\triangle$, where $\hat{N}_\triangle$ is the total electron number operator for all sites in the triangular lattice. $\hat{H}_\triangle(\mu)$ is designed such that the lowest two bands will be of the honeycomb (triangular) character when $\mu=0$ ($\mu=1$). The interpolating Hamiltonian is then defined as $\hat{H}(\mu)\equiv\hat{H}_0+\hat{H}_{c(\mu)}+\hat{H}_\triangle(\mu)$.

The band gap of $\hat{H}(\mu)$ at filling 2 is shown in Supplemental Fig. 1b. The gap never vanishes, and attains a minimum in

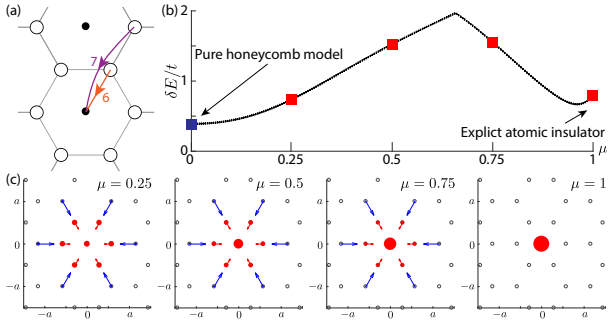

Supplemental Figure 1. **Adiabatic deformation to an atomic limit.** (a) Coupling between the honeycomb sites and additional sites at the centers of the hexagons. (b) Symmetric smooth deformation of the pure honeycomb groundstate ($\mu=0$) to an explicit atomic insulator with electrons localized to the centers of the hexagons ($\mu=1$). δE denotes the band gap at filling 2. A cross indicates a data point computed using ~ 1350 points along the path in Fig. 1b in the main text together with an additional 10^5 random points in the Brillouin zone. (c) Smooth evolution of the Wannier functions for μ indicated by the four red squares in (b). See Fig. 1c in the main text for the Wannier function in the pure honeycomb limit (blue square), and a description on how it is visualized.

the purely honeycomb limit ($\mu = 0$). This corresponds to a symmetric, adiabatic deformation between the groundstate of $\hat{H}_0$ and an explicit atomic insulator. We further visualize the Wannier functions as a function of μ in Supplemental Fig. 1c, showing their expected smooth evolution.

III. CONSTRUCTING WANNIER FUNCTIONS

We will use the "projection method" to construct symmetric, well-localized Wannier functions [39, 40]. The method proceeds by first specifying a collection of well-localized, symmetric wavefunctions in real space, which serves as a reasonable guess for the actual Wannier functions. These trial wavefunctions are then projected into the valence-band subspace to determine a collection of unitaries which correspond to a "smooth gauge" for forming well-localized Wannier functions. In this process, at every $\boldsymbol{k}$ we have a Hermitian matrix $S_{\boldsymbol{k}}$ quantifying the overlap between our initial seeds and the actual valence bands. The projection procedure is well-defined and gives well-localized Wannier functions when $\det S_{\boldsymbol{k}} > 0\ \forall \boldsymbol{k}$. Failure of which for all choices of symmetric, well-localized trial wavefunctions is generally believed to be a sign of a topological band structure [16, 17]. In practice, one keeps track of the stability of the procedure by monitoring the size of $\det S_{\boldsymbol{k}}$ across the BZ, which could be achieved by ensuring the ratio $\max_{\boldsymbol{k}}\{\det S_k\}/\min_{\boldsymbol{k}}\{\det S_k\}$ does not diverge [39]. In addition, using the ideas in Ref. 40, one can verify that as long as $\det S_k > 0$ for all $\boldsymbol{k}$, the resulting Wannier functions will inherit the symmetry properties of the trial ones.

For our problem, we will construct the symmetric Wannier functions of $\hat{H}_0$ using the smooth deformation $\{\hat{H}(\mu) : \mu \in [0, 1]\}$ we discussed. Of course, the existence of symmetric, exponentially localized Wannier function is independent of the method one uses to find them, so if one prefers, one can also construct the desired Wannier functions for $\hat{H}_0$ without ever introducing the additional triangular sites. Our construction proceeds as follows: We start with the Wannier functions for $\hat{H}(1)$, which are simply the p_z orbitals localized to the triangular sites. We then use these as the trial wavefunctions to find the Wannier functions of $\hat{H}(\mu')$ for some $\mu' < 1$. These new Wannier functions are then used as the trials for some $\mu'' < \mu'$. We do this iteratively until we arrive at $\mu = 0$, resulting in the Wannier functions for the pure honeycomb model $\hat{H}_0$. Numerically, we simply perform this procedure for the values of μ indicated by red squares in Supplemental Fig. 1b. The Wannier functions are computed using a 200×200 regular momentum mesh for the BZ. On top of that, we evaluate $S_{\boldsymbol{k}}$ for an additional 3×10^4 randomly sampled momenta. As μ parameterizes a symmetric smooth deformation of the groundstate wave function, we expect the projection to proceed without obstruction at every step in the construction. This can be verified from the behavior of $\det S_{\boldsymbol{k}}$ along the projection, as tabulated in Supplemental Table II.

Note that no obstruction is encountered as we successively project the initial, tightly localized trial wavefunctions (using a finite number of steps) to obtain the symmetric Wannier functions of the honeycomb model $\hat{H}_0$. This is strongly indicative that the our Wannier functions are exponentially localized. We will not attempt to prove this in an analytic manner here; rather, we simply point to the numerical evidence that the found Wannier functions decay with an envelope which is clearly exponentially decaying.

Finally, we comment that spin-orbit coupling plays a crucial role in the existence of the symmetric, exponentially localized Wannier functions. This is reflected in a nontrivial phase winding of the wavefunction, locked to the in-plane spin component, as one circles the charge center. One can readily derive the required locking patterns by, e.g., writing down wavefunctions which are compactly supported on the six vertices of a hexagon and transforming in the stipulated way. Of course, such a wavefunction does not automatically satisfy the orthogonality condition with its translation copies, and therefore cannot be immediately interpreted as the Wannier functions of some parent Hamiltonian. Nonetheless, it captures the essence of the symmetry properties required, and, if preferred, one can as well use it as a trial wavefunction for finding the Wannier functions [39, 40] of the valence bands of $\hat{H}_0$.

Supplemental Table II. **Data on the construction of Wannier functions through successive projections along the smooth deformation parameterized by μ.** We follow the notation in Ref. 39 for the overlap $S_{\boldsymbol{k}}$, the gauge-invariant spread functional Ω_{I}, and the gauge-dependent one $\tilde{\Omega}$. a denotes the lattice constant.

μ	0.75	0.5	0.25	0.00
$\min_{\boldsymbol{k}}\{\det S_{\boldsymbol{k}}\}$	0.27	0.85	0.83	0.74
$\max_{\boldsymbol{k}}\{\det S_{\boldsymbol{k}}\}/\min_{\boldsymbol{k}}\{\det S_{\boldsymbol{k}}\}$	1.53	1.09	1.08	1.05
Ω_{I}/a^2	0.38	0.68	1.01	1.20
$\tilde{\Omega}/a^2$	0.00	0.01	0.02	0.03

IV. A MORE PHYSICAL VIEW ON FRAGILE TOPOLOGY

While we have already provided a precise definition of fragile topology, it is helpful to shift the perspective from a more mathematical point of view to a physical one, concerned not with the topology of an isolated set of bands, but that of a band insulator: Consider placing the set of bands whose topology is to be determined at the bottom of the spectrum, and place the chemical potential above them so that they are the only filled bands. We will allow for the addition of *any* extra degrees of freedom *above* the Fermi level. This is rather physical—a bounded tight-binding model is only an approximation to any physical problem, and so it is unreasonable to forbid the addition of high-energy orbitals in the discussion. Now, we ask if we can tune some parameters and deform the system into an explicit atomic insulator, while preserving the band gap and symmetries throughout. If yes, then we conclude the valence bands, our target set, are trivial; if no, then they are topological, and we have to further discern if the topology is stable or fragile. These two cases can be differentiated by further

stacking with atomic insulators, corresponding to the addition of trivial bands below the Fermi level, and then ask if the new set of valence bands is adiabatically and symmetrically deformable into an atomic limit. We conclude our target set possesses fragile topology if and only if such a deformation is possible for some choice of additional trivial bands.

V. K-THEORY AND FRAGILE TOPOLOGY

Here, we provide a slightly more formal discussion on how the notion of fragile topology is inspired by the notion of stable equivalence in K-theory. To this end, we first introduce some ideas from the K-theory-based classifications of band insulators [1, 9–13]. Note that the following serves only as a brief introduction, and we refer the readers to the references above for a mathematically precise discussion.

Suppose there is a topological obstruction in deforming between band insulators a and b without either closing the band gap or allowing symmetry breaking in the process. In equation, we may write $a \not\sim b$. However, it could be the case that the obstruction is resolved once we stack some additional band insulator c with both a and b, i.e., $a \oplus c \sim b \oplus c$ (Fig. 2a in the main text). From a physical point of view, c may be an atomic insulator corresponding to some closed-shell electrons tightly localized to the underlying atoms. Since the deformation obstruction could be resolved by mixing with degrees of freedom that are buried deep below the Fermi energy, it is natural on physical grounds to disregard such apparent distinctions. Mathematically, one say a and b are "stably equivalent," and write $a \sim_{\mathrm{s}} b$.

The discussion above closely mirrors the key physical aspects of the notion of "fragile" vs. "stable" topology. Suppose a set of bands FT is topological in the sense that, for any trivial (i.e., atomic) band insulator t, $\mathrm{FT} \not\sim \mathrm{t}$. Now we say FT has fragile topology if one can find some trivial t', t'' such that $\mathrm{FT} \oplus \mathrm{t}' \sim \mathrm{t}''$ (Fig. 2b in the main text), and we say it is stably topological otherwise (Fig. 2c in the main text).

In closing, we note that the K-theory-based classifications of band insulators [1, 9–13] are designed to (only) capture stable topological distinctions between band insulators, and therefore it does not automatically incorporate our present notion of triviality, which is defined with respect to Wannier representability. As an example, the number of occupied bands is a topological invariant in the K-theory sense, since there is no way to deform a set of N bands into N' bands when $N \neq N'$. For physics applications, however, the electron filling in a band insulator is usually irrelevant to discussions for topological band insulators, as one can typically find a full set of atomic insulators which realizes all the possible band-insulator fillings (We note in passing that, assuming either spinful or spinless fermions, the only exceptions to this rule (in the stable sense) among the 1,651 magnetic space groups were identified in Refs. 18 and 53. These are instances where the stable band topology is manifested already in the electron filling.) Our present notion of triviality of a band insulator, which is based on the existence of an atomic description, can be introduced into the K-theory framework by identifying the atomic-insulator subgroup in the full classification [18, 53].

VI. BAND REPRESENTATIONS

To be self-contained, we provide here a very brief introduction to the notion of "band representations" [42–45]. For details, please refer to Refs. 19, 27, and 28, and the references therein.

Loosely, a band representation is specified by two pieces of data: (i) the positions of the sites at which the electronic degrees of freedom reside, and (ii) how the local energy levels transform under the subgroup of the SG which leaves a site invariant. In addition, band representations can be "added," which corresponds physically to the stacking of the local energy levels. Given a band representation, one can ask if it can be regarded as a stack of smaller ones, each involving fewer energy levels than the original. Whenever such an interpretation is possible, we say the band representation is "composite." Any band representation which is not composite is called "elementary."

As defined, EBRs are the building blocks which generate all possible tightly localized atomic insulators under the stacking operation [43–45]. Following the terminology in Refs. 19, 27, and 28, we refer to a time-reversal symmetric EBR as a "physical" EBR (PEBR). Note that all the PEBRs we discuss in this work are also EBRs [19, 27], and hence we refrain from complicating the discussion by considering PEBRs in details. Generally, it is possible that the energy bands corresponding to a (P)EBR can be split into valence and conduction bands separated by a band gap. When this is possible, we say the (P)EBR is decomposable [19, 27, 28].